MATERIALS CHEMISTRY FRONTIERS

RESEARCH ARTICLE

View Article Online
View Journal | View Issue

Cite this: *Mater. Chem. Front.*, 2022, **6**, 3555

Assembling ionic liquids in MOF "Monomer" based membranes to trigger CO_2/CH_4 separation†

Xiaolei Cui,‡[a] Zixi Kang,‡*[bc] Weidong Fan,[b] Jia Pang,[b] Yang Feng,[a] Caiyan Zhang,[b] Liting Yu,[b] Shuo Liu,[b] Xiuxian Tang,[b] Lili Fan,[b] Rongming Wang[b] and Daofeng Sun*[b]

Received 8th August 2022,
Accepted 5th October 2022

DOI: 10.1039/d2qm00802e

rsc.li/frontiers-materials

The advantages of ionic liquids (ILs) in the selective adsorption of CO_2 can improve the CO_2-selective separation performance of IL-modified membranes. Herein, a facile post-modification strategy using ILs has been developed for filling the interspace of MOF "monomer" based membranes to enhance the CO_2/CH_4 sieving performance. The membranes constructed *via* the interfacial polymerization of MOF "porous monomers" and trimesoyl chloride (TMC) have nanoscale interspaces, which limit the performance of these membranes in the field of precise CO_2/CH_4 sieving. The addition of ILs with high CO_2 affinity filled these interspaces between the MOF and TMC monomers, resulting in a CO_2/CH_4 selectivity of 35 for the modified membranes compared with the non-selectivity of the pristine membrane. Furthermore, the hydrogen-bond interaction between ILs and the membrane improves the separation stability and avoids the loss of ILs during gas permeation. After long-term continuous gas separation tests, the membrane can maintain stable CO_2/CH_4 selectivity. Therefore, a post-modification membrane using ILs is highly desirable for enhancing the gas separation performance of MOF "porous monomer" based membranes for natural gas purification applications.

1. Introduction

Natural gas is considered a primary fuel source with a high H/C ratio and low emission of pollutants in comparison to oil and coal. In addition to the main component methane (CH_4), natural gas also contains a large amount of acid gases, such as carbon dioxide (CO_2), which need to be removed before it enters the pipeline. Therefore, efficient separation of CO_2 from CH_4 is necessary and has gained significant attention.[1–4] Traditional CO_2 purification technologies are amine scrubbing and pressure swing adsorption, which are complex and energy-intensive processes.[5] Membrane-based separation technology requires less cost and energy consumption and is more environmentally friendly.[6–8] In principle, membrane materials with excellent selectivity, permeability, and stability are the keys to achieving efficient gas separation.

Metal–organic framework (MOF) membranes, as emerging membrane materials, have been extensively studied because of their adjustable pore size, designable structure, and high porosity, which can ensure precise and efficient separation of CO_2.[9,10] Nevertheless, the brittleness and synthesis conditions of stable MOFs make it difficult to fabricate scalable and defect-free polycrystalline membranes for efficient separation. To overcome the issues of polycrystalline membranes, MOFs have been combined with polymers to construct mixed matrix membranes (MMMs).[11–14] However, the good compatibility of the two species, low membrane thickness, and homogeneous dispersion of high proportions of fillers should be realized to trigger the ideal separation performance.

To address these points, in the previous work, we applied ultra-small amino-functionalized MOFs as "porous monomers" to interfacially polymerize with trimesoyl chloride (TMC), forming flexible composite membranes within 10 minutes.[15] Due to the low membrane thickness (150 nm) and high MOF loading (>55%), the membranes possess a high water permeance of 55.9 L m^{-2} h^{-1} bar^{-1} and a dye rejection of 99.8% for nanofiltration application and can maintain the performance after being scaled up. This strategy for preparing flexible, high filler proportion, ultra-thin and scalable MOF membranes can also be expanded to other crystalline porous materials. Although the

[a] *College of Chemical and Chemical Engineering, China University of Petroleum (East China), Qingdao, Shandong, 266580, P. R. China*
[b] *College of Science, School of Materials Science and Engineering, China University of Petroleum (East China), Qingdao, Shandong, 266580, P. R. China. E-mail: kzx@upc.edu.cn, dfsun@upc.edu.cn*
[c] *State Key Laboratory of Structural Chemistry, Fujian Institute of Research on the Structure of Matter, Chinese Academy of Sciences, Fuzhou, Fujian, 350002, P. R. China*

† Electronic supplementary information (ESI) available. See DOI: https://doi.org/10.1039/d2qm00802e

‡ These authors contributed equally to this work.

membranes prepared using this strategy have effective retention of dyes, the pore size of 1.15 nm between monomers is not suitable for the separation of smaller gas molecules such as CO_2 (dynamic diameter of 0.33 nm).[15] To expand the application of these flexible membranes for gas separation, tailoring the interspace between monomers and enhancing adsorption selectivity may be beneficial to improve the gas permeation selectivity.

Inspired by the method of repairing defects in polycrystalline membranes, other substances have been covered on the membrane to eliminate or minimize boundary defects.[16] In the pioneering works, Pan *et al.* prepared a ZIF-8 crystalline membrane on tubular ceramic support and deposited PDMS on the membrane surface.[17] The coating of PDMS can effectively repair the inter-crystalline defects of the ZIF-8 membrane and significantly improve the quality and reproducibility of the synthesized membranes. Zhou *et al.* repaired defective zeolite membranes using a siloxane polymer coating with the imidazole group *via* chemical liquid deposition.[18] The modified membrane showed an increased CO_2/CH_4 selectivity by one order of magnitude and a slightly decreased CO_2 permeance by less than 25%. In this regard, the post-modification of membranes is an effective strategy to seal the defects and improve the molecular sieving effect.

Ionic liquids (ILs) are salts that are liquids at room temperature and have advantages over traditional solvents such as high chemical and thermal stability, high polarity, and low volatility.[19–21] The charge of some ILs can physically interact with the quadrupole moment of CO_2 molecules, thus, ILs have become promising CO_2 capture solvents.[22,23] In previous MOF-based membranes, ILs have also been proved to be potentially guest molecules for CO_2 capture. Yang *et al.* assembled ILs into the cavities of ZIF-8 resulting in a reduced pore size.[24] ZIF-8@IL was used as the filler for MMMs, which effectively improved the CO_2 screening performance. From this perspective, ILs can not only reduce the pore size of the membranes but also acts as a CO_2 affinity agent to improve their CO_2 capture capacity. Although IL-modified membranes exhibit superior properties, there is still a great challenge to resolve the problem of losing ILs easily from the membrane, which may cause degraded performance during long-time separation.

In this work, a facile post-modification strategy for optimizing the gas separation performance of MOF-based composite membranes by introducing ILs was proposed (Scheme 1). First, the ultra-small particles of the MOF (UiO-66-NH_2) were used as "porous monomers" to covalently bond with an acid chloride monomer (TMC) through the classic and scalable interfacial polymerization process without other amine monomers, forming UiO-66-NH_2-TMC membranes. Then ILs (1-butyl-3-methylimidazole bis(trifluoromethanesulfonyl)imide, [BMIM]TF_2N) with high CO_2 affinity were filled in the UiO-66-NH_2-TMC membranes to seal the voids and narrow the pore size. Furthermore, the F atoms in ILs can form hydrogen bonds with H atoms from $-NH_2$ and –COOH in the membranes, which solves the problem of IL loss and improves the separation stability. These MOF-based composite membranes after IL modification exhibited a CO_2/

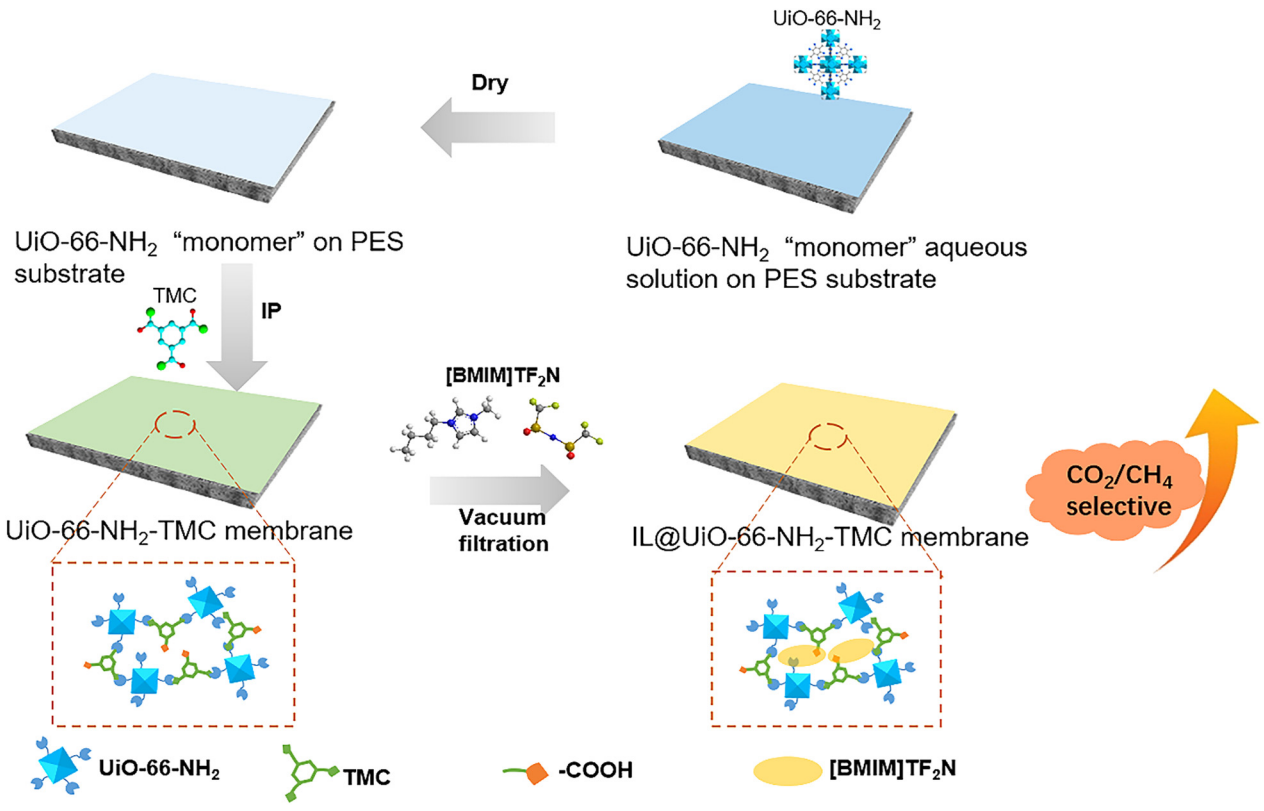

Scheme 1 Preparation of the IL@UiO-66-NH_2-TMC membrane.

CH_4 selectivity of 35 compared with the non-selective pristine membrane. The high selectivity remains unchanged even after 1440-minutes of continuous gas separation testing. The combination of a scalable "porous monomer" interfacial assembly strategy and IL post-modification provides a new opportunity to construct composite membranes for efficient gas separation.

2. Experimental

2.1 Materials

Zirconium(IV) chloride ($ZrCl_4$, Strem Chemicals, 99.95%), 2-aminoterephthalic acid ($H_2BDC\text{-}NH_2$, Energy Chemical, 98%), *N*,*N*-dimethylformamide (DMF, Sinopharm Chemical Reagent, >99.5%), 1,3,5-benzenetricarbonyl trichloride (TMC, Sigma-Aldrich, 98%), cyclohexane (C_6H_{12}, FHUYU Chemical, >98%), methanol (CH_3OH, Sinopharm Chemical Reagent, >99.5%), and 1-butyl-3-methylimidazole bis(trifluoromethanesulfonyl)imide salt ([BMIM]TF_2N, Energy Chemical, 98%) were employed in this study.

2.2 Preparation of UiO-66-NH_2 "porous monomers"

UiO-66-NH_2 was synthesized according to the reported literature.[25] Typically, 0.65 g of $ZrCl_4$, 0.48 g of 2-aminoterephthalic acid, and 7.56 g of deionized water were added to 160 mL of DMF. The mixture was ultrasonically dissolved and then heated at 120 °C for 24 h. After the solution was cooled to room temperature, the product was collected by centrifugation and washed with DMF (15 mL × 5) and deionized water (15 mL × 8). The UiO-66-NH_2 solid (yield = 79%) was collected for later use.

2.3 Interfacial polymerization of the UiO-66-NH_2-TMC membrane

PES ultrafiltration membranes (pore size: 100 nm) were used as the substrates of composite membranes. The UiO-66-NH_2 was diluted with deionized water to prepare 0.05 wt% aqueous dispersions of the UiO-66-NH_2 monomer. In our previous work, the optimal concentration of UiO-66-NH_2 aqueous dispersions and the interfacial polymerization time have been systematically explored.[15] When the MOF monomer concentration was 0.05 wt% and the interfacial polymerization time was 5 min, the obtained membrane material was continuous, dense, and has good performance. Therefore, in this study, 0.05 wt% aqueous dispersions of the UiO-66-NH_2 were selected for the preparation of UiO-66-NH_2-TMC membranes. For the interfacial polymerization, first, the PES substrate was soaked in the aqueous dispersion of UiO-66-NH_2 monomers for 10 s, then taken out and fixed on a self-made mold. The wet PES substrate was dried with a 50 °C hot lamp to ensure that enough MOF monomers remained on the substrate. Then 0.5 wt% TMC cyclohexane solution was gently poured into the mold. After 10 min of interfacial polymerization at room temperature, the TMC cyclohexane solution was discarded, and the UiO-66-NH_2-TMC membrane was washed with pure cyclohexane three times to remove excess TMC. Here, in order to further increase the crosslinking degree of the membrane, the time of interfacial polymerization was extended to 10 min. Finally, the UiO-66-NH_2-TMC membranes were heated under a hot lamp at 50 °C for 5 min to ensure that the polymerization reaction was complete.

2.4 IL@UiO-66-NH_2-TMC membrane after post-modification

After the UiO-66-NH_2-TMC membranes were prepared, [BMIM]-TF_2N ILs were assembled in the membranes to seal the voids and narrow the pore size. The ionic liquid of [BMIM]TF_2N was selected due to its excellent CO_2 affinity and solubility, and its hydrogen bonding interaction with the UiO-66-NH_2-TMC membranes. The UiO-66-NH_2-TMC membranes were fixed in the vacuum filtration device, and the methanol solution of IL (10 mL) with varying concentrations (10 wt%, 15 wt%, and 20 wt%) was poured onto the composite membranes, and the vacuum filtration time was 10 min. Then the membranes were heated at 50 °C for 30 min to evaporate the methanol solvent. The obtained UiO-66-NH_2-TMC membranes and IL@UiO-66-NH_2-TMC membranes prepared with IL concentrations of 10 wt%, 15 wt%, and 20 wt% were named M0, M1, M2, and M3, respectively (Table 1). After the filtration, the IL methanol solution in the vacuum filter bottle was collected. After the evaporation of methanol, the unmodified IL content was measured to calculate the amount of IL in membranes (Table 1).

2.5 Characterization

The chemical structures of the resultant membranes were characterized using a Fourier transform infrared spectrophotometer (FTIR, IRTracer-100, SHIMADZU). X-ray photoelectron spectroscopy (XPS, Thermo ESCALAB 250, SHIMADZU) was used to further investigate the chemical composition of the resultant membranes. The structures of the resultant membranes and UiO-66-NH_2 powder were examined with X-ray diffraction (XRD, XRD-6000, SHIMADZU) at a scanning rate of 10° min^{-1} and 5–50° angular range. The surface and cross-sectional morphologies of the resultant membranes were collected using a scanning electron microscope (SEM, JSM-7900F, JEOL). The Brunauer–Emmett–Teller (BET) surface area and the pore size distributions of UiO-66-NH_2 were calculated based on the N_2 adsorption–desorption isotherms at 77 K collected with a Micromeritics ASAP 2020. The CO_2 and CH_4 adsorption isotherms for the UiO-66-NH_2-TMC membrane and IL@UiO-66-NH_2-TMC membranes were measured with the Micromeritics ASAP-2020 surface area analyzer at a temperature of 298 K. Thermogravimetric analysis (TGA) was performed using a TGA STAR^e system under a nitrogen atmosphere.

2.6 Gas separation experiment

The single and mixed gas permeation tests were performed with Wicke–Kallenbach apparatus. The membranes were fed

Table 1 Synthesis conditions of different membranes

Membrane ID	UiO-66-NH_2 dispersions (wt%)	TMC solution (wt%)	IL solution (wt%)	IL content (g)
M0	0.05	0.5	0	0
M1	0.05	0.5	10	0.2
M2	0.05	0.5	15	0.36
M3	0.05	0.5	20	0.47
M_{PES+IL}	0	0	15	0.12

with single (CO_2 and CH_4, purities of 99.99%) and mixed (CO_2/CH_4 = 1 : 1, v/v) gas in the pressure range of 1.2–2.0 bar, while the permeate side was kept at atmospheric pressure. Single gas with a flow rate of 100 mL min^{-1}, or a CO_2/CH_4 mixture gas with a total flow rate of 100 mL min^{-1} was used as the feed gas, and argon with a flow rate of 40 mL min^{-1} was used as the sweep gas. The permeance (P_i, GPU, 1 GPU = 3.3928 × 10^{-10} mol m^{-2} s^{-1} Pa^{-1}) of the membranes was calculated using eqn (1):[24,25]

$$P_i = \frac{N_i}{\Delta p_i \times A} \quad (1)$$

where N_i (mol s^{-1}) is the permeate flow rate of component i, interval, Δp_i (Pa) is the transmembrane pressure drop of i, and A (m^2) is the membrane area.

For single gas separation, the ideal gas selectivity ($\alpha_{i,j}$) is obtained according to eqn (2):

$$\alpha_{i,j} = \frac{P_i}{P_j} \quad (2)$$

where P_i and P_j represent the permeance of components i and j.

For mixed gas separation, the separation factor (S.F.) is obtained according to eqn (3):

$$\text{S.F.} = \frac{X_i/X_j}{Y_i/Y_j} \quad (3)$$

where i, j represent the two components in the mixture and X, Y are the mole fractions in the permeate and feed gas, respectively.

The solution-diffusion model was applied to study the gas permeance through the IL@UiO-66-NH_2-TMC membranes. The calculation formula is shown in eqn (4):[26,27]

$$P_i l = S_i \times D_i \quad (4)$$

where the permeability ($P_i l$) is equal to the product of the solubility (S_i, mol m^{-3} Pa^{-1}) and the diffusivity (D_i, m^2 s^{-1}), and l is the thickness of membranes. The ideal selectivity (ideal $\alpha_{i,j}$) of the pure gas was calculated using eqn (5):[28]

$$\alpha_{i,j} = \left(\frac{S_i}{S_j}\right) \times \left(\frac{D_i}{D_j}\right) \quad (5)$$

The S_i can be calculated by eqn (6):

$$S_i = \frac{C_i}{P} \quad (6)$$

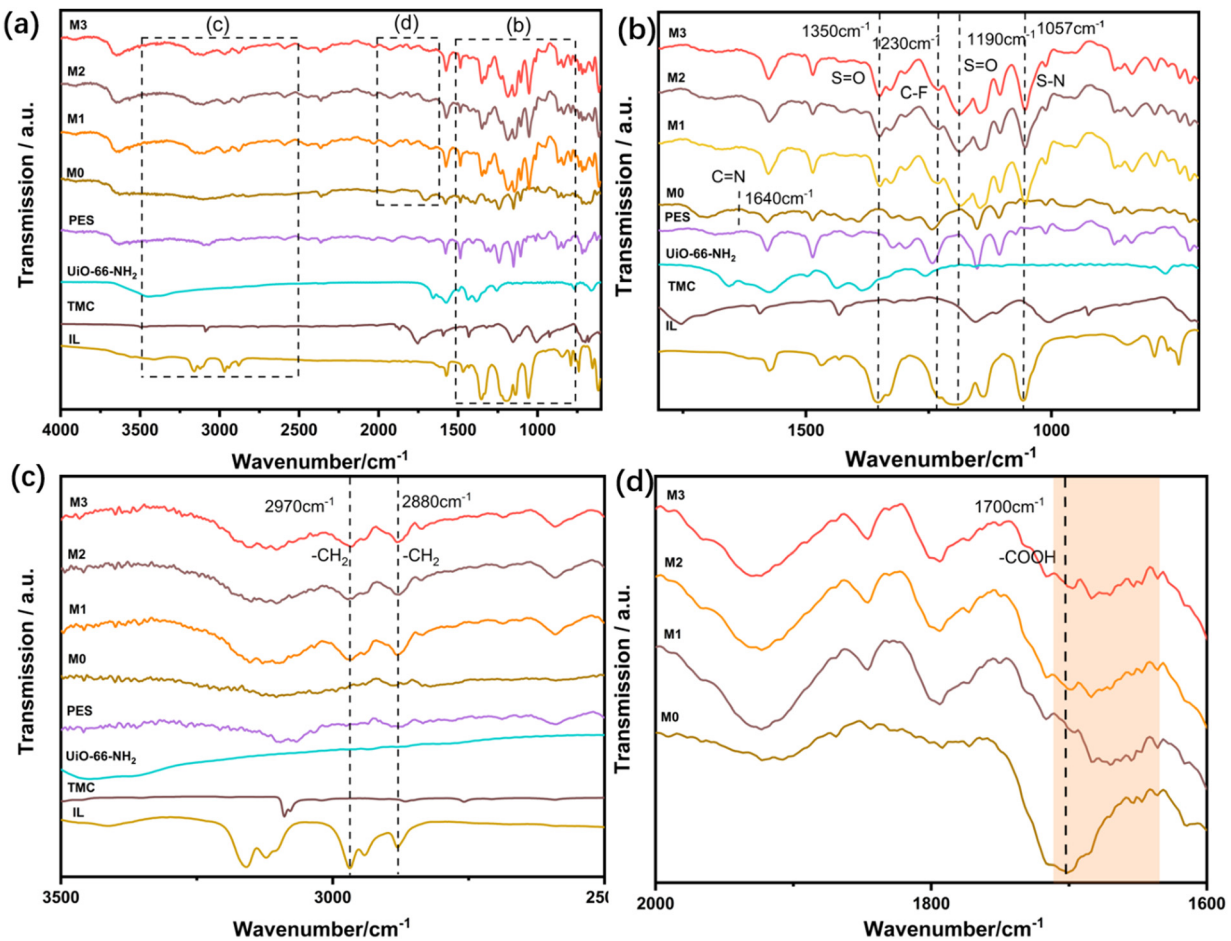

Fig. 1 (a) The FT-IR spectra of IL, TMC, UiO-66-NH_2, PES substrate, UiO-66-NH_2-TMC membrane (M0), and IL@UiO-66-NH_2-TMC membranes prepared with IL concentration of 10 wt%, 15 wt%, and 20 wt% (M1–M3); (b–d) the magnified parts of (b–d) in (a).

where C_i (mmol cm^{-3}) and P are the adsorption amount of the membrane for component i and pressure, respectively. D_i was calculated according to eqn (4).

3. Results and discussion

3.1 Membrane characterization

The chemical groups of IL, TMC, UiO-66-NH_2, PES substrate, and synthesized membranes were detected using FTIR spectroscopy. Fig. 1(b–d) show the magnified parts of (b–d) in Fig. 1(a). In the IR spectrum of the M0 membrane (Fig. 1b), the peak that appears at 1640 cm^{-1} is associated with the stretching vibration of C═N,[29] indicating that UiO-66-NH_2 and TMC are covalently linked to the amino group. The characteristic peaks of M1–M3 membranes at 1350, 1230, 1190, and 1057 cm^{-1} were ascribed to the S═O asymmetric stretching, C–F asymmetric stretching, S═O symmetric stretching, and S–N asymmetric stretching of [TF_2N] (—) in ionic liquids, respectively (Fig. 1b).[22] The bands at 2880 cm^{-1} and 2970 cm^{-1} in Fig. 1c can be assigned to the symmetric and asymmetric extension of the –CH_2– group in the [BMIM] (+) alkyl chain.[30–32] These results confirmed the successful loading of ILs into M1–M3. Compared with M0, the –COOH characteristic peak of M1–M3 membranes shifted from 1700 cm^{-1} to 1670 cm^{-1} (Fig. 1d), which indicates the hydrogen bonding between the H atom from –NH_2 and –COOH in the membrane and F atom in [BMIM] TF_2N.

The newly formed chemical composition within the synthesized membrane before and after IL assembly can be characterized by XPS technology (Fig. 2). The peaks of C 1s (285 eV), O 1s (532 eV), N 1s (399.6 eV), and Zr 3d (182 eV) were observed in the wide scanning spectra of both UiO-66-NH_2-TMC and IL@UiO-66-NH_2-TMC membranes.[33,34] Compared with the UiO-66-NH_2-TMC membrane, a new peak (169 eV) appeared in the spectrum of the IL@UiO-66-NH_2-TMC membrane, which belongs to the S element in [BMIM]TF_2N.[35] To analyze the chemical state clearly, the XPS C 1s and N 1s spectra of membranes before and after ILs assembly were recorded (Fig. 2b and c). In Fig. 2b, the peaks of the UiO-66-NH_2-TMC membrane at 285 eV (Peak 1) are associated with C–C, C–H, and C–N functional groups.[36] The peaks of the IL@UiO-66-NH_2-TMC membrane at 285 eV (Peak 1) can be attributed to C–C, C–H bonds, 286.5 eV (Peak 2) correspond to the C–N bond, and 293 eV (Peak 3) correspond to –CF_3 groups respectively.[37–39] The presence of –CF_3 groups in the IL@UiO-66-NH_2-TMC membrane mainly comes from [TF_2N] (−). Besides, the area corresponding to the C–N bond for the IL@UiO-66-NH_2-TMC membrane increases compared to the UiO-66-NH_2-TMC membrane, which was due to the immobilization of [BMIM] (+) between UiO-66-NH_2 and TMC.[40,41] The N 1s spectrum of the UiO-66-NH_2-TMC membrane shows a broad peak at 399.6 eV (Peak 1) (Fig. 2), corresponding to the N–C and N–H bonds within the membrane. Two characteristic peaks appeared in the N 1s spectrum of the IL@UiO-66-NH_2-TMC membrane at 399.6 eV (peak 1) and 402.5 eV (peak 2). Peak 1 corresponds to the N–C bond and N–H bonds in the membrane and the N element in [TF_2N] (−), and peak 2 corresponds to the two N atoms in the imidazole ring of [BMIM] (+). The results provide further evidence for the successful confinement of ILs into the membrane.

The XRD patterns of the UiO-66-NH_2 powder and prepared membranes are shown in Fig. 3a. The XRD patterns of synthesized UiO-66-NH_2 fitted well with the simulated patterns, demonstrating that the targeted structure was constructed. The characteristic peaks of UiO-66-NH_2 at 7.3° and 8.4° are relatively broad, which is caused by the ultra-small particle size for UiO-66-NH_2. To further clarify the pore structure of the MOF, the N_2 adsorption isotherm (BET data) of the synthesized ultra-small UiO-66-NH_2 was tested (Fig. S1, ESI†). The N_2 adsorption results demonstrate that UiO-66-NH_2 possesses a BET surface area of 373 m^2 g^{-1} and follows a class IV adsorption curve (Fig. S1a, ESI†). There is a hysteresis loop in the middle part of the adsorption curve.[42] The reason for this phenomenon is that the particle size of UiO-66-NH_2 is too small, and it is easy to agglomerate together and generate intercrystalline mesopores. This phenomenon can also explain the inhomogeneity of the pore size distribution of UiO-66-NH_2, as shown in Fig. S1b (ESI†). The pore size distribution at 7 Å and 11 Å belong to the pore window and pore cavity of UiO-66-NH_2, respectively, while the pores larger than 11 Å are intercrystalline pores generated by the agglomeration of MOFs. These results combined with the XRD patterns demonstrate the successful formation of the porous MOF structures. Moreover, the available amine groups inside the synthesized UiO-66-NH_2 were quantified using XPS analysis, as shown in Fig. S2 (ESI†). The peaks of UiO-66-NH_2 were observed

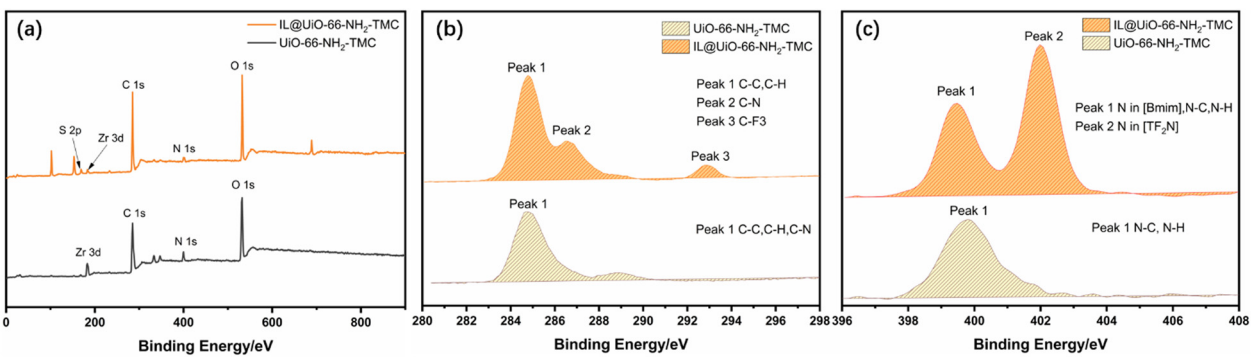

Fig. 2 XPS spectrum of (a) UiO-66-NH_2-TMC and IL@UiO-66-NH_2-TMC membranes, (b) C 1s for UiO-66-NH_2-TMC and IL@UiO-66-NH_2-TMC membranes, (c) N 1s UiO-66-NH_2-TMC and IL@UiO-66-NH_2-TMC membranes.

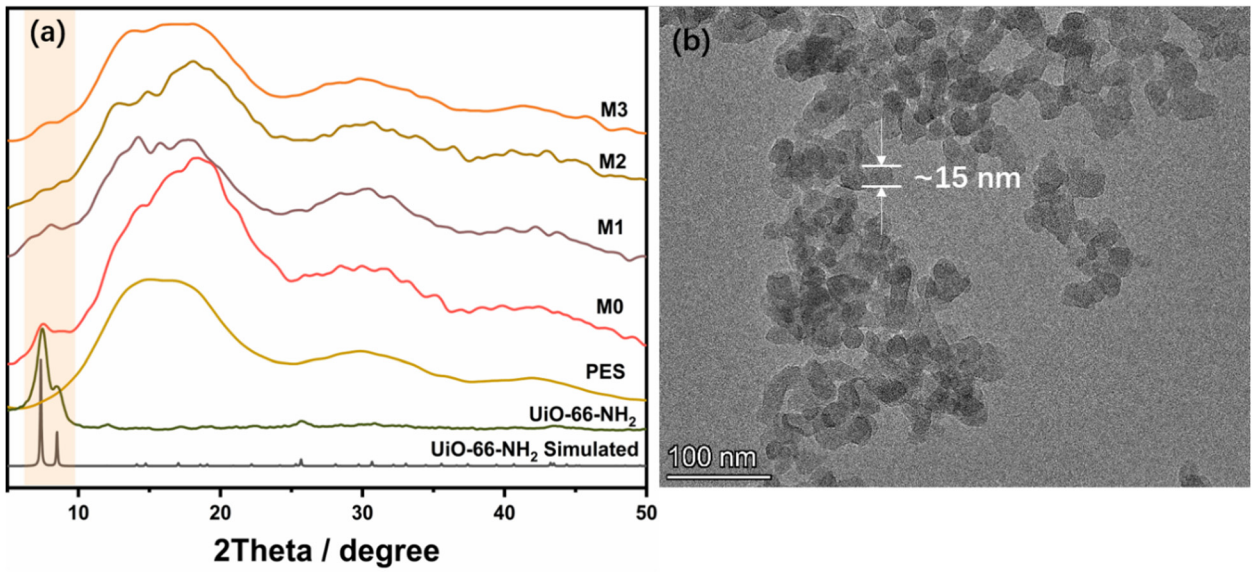

Fig. 3 (a) XRD patterns of UiO-66-NH_2 simulated, UiO-66-NH_2, PES substrate, and M0–M3. (b) TEM of the L-UiO-66-NH_2.

for C 1s (285 eV), O 1s (532 eV), N 1s (400 eV), and Zr 3d (182 eV) in the wide-scan spectra. Among them, the proportion of N element is 6.4%, suggesting that the amine content in UiO-66-NH_2 is high. UiO-66-NH_2 is formed by the coordination of the $Zr_6O_4(OH)_4$ cluster with 2-aminoterephthalic acid. Each ligand contains an amino group, so each structural unit of the formed UiO-66-NH_2 contains amino functional groups, and the surface ones can link with TMC during the interfacial polymerization process. The TEM image (Fig. 3b) reveals that the particle size of UiO-66-NH_2 "monomers" is 16 nm. Furthermore, M0–M3 all showed diffraction peaks in the range of 7.3–8.4°, proving that the crystal structure of UiO-66-NH_2 in the composite membranes was retained (Fig. 3a).

After confirming the material structures, the morphologies of the PES substrate, M0–M3, were observed in the SEM images. As shown in Fig. 4, the PES substrate has many voids with a size of ~100 nm. By contrast, after the synthesis of membranes by interfacial polymerization (Fig. 5a), the substrate is completely covered with a continuous selective layer. The larger pore size and hydrophilicity of the PES substrate can effectively retain the UiO-66-NH_2 monomer, which lays a foundation for the interfacial polymerization of membranes. M1–M3 membranes exhibit continuous surfaces without obvious defects (Fig. 5b–d). When the IL concentration was up to 20 wt%, excess IL could be observed on the membrane surface. It can be seen from the cross-sectional image of the membrane that the thickness of the IL@UiO-66-NH_2-TMC membrane is about 150 nm (Fig. 5f–h), and the addition of IL does not significantly increase the thickness of the original membrane (Fig. 5e), indicating that IL is mainly assembled into the membrane rather than being deposited on the surface.

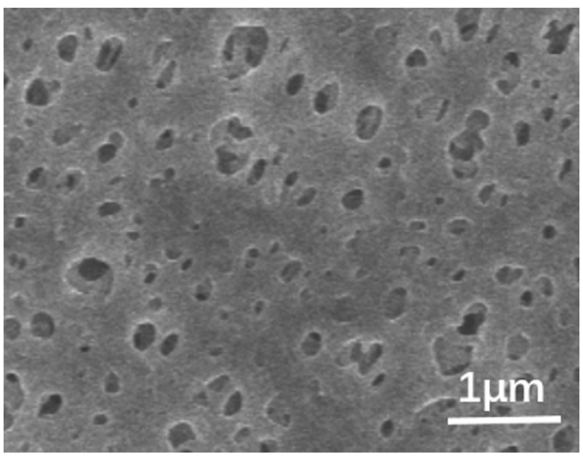

Fig. 4 The top-view SEM images of the PES substrate.

To clarify the distribution of UiO-66-NH_2 on the PES substrate, we have collected a cross-sectional SEM image of the UiO-66-NH_2-TMC membrane and an EDS mapping image of the IL@UiO-66-NH_2-TMC membrane. (Fig. S3, ESI†). The size of the UiO-66-NH_2 particles (~20 nm) is smaller than that of the PES substrate (100 nm), so after the PES soaks the MOF aqueous phase, some UiO-66-NH_2 particles will enter the inside of the PES pores, and these particles will aggregate inside the PES pores (Fig. S3a, ESI†), but these MOF particles are few and discontinuous, which have no influence on the separation performance. Beyond the MOF particles inside the PES pores, a uniform UiO-66-NH_2 layer is spread on the surface of the PES, and the membrane formed in this part can be visually observed by SEM. Compared with the membrane layer formed on the PES surface, the scattered MOF particles in the PES pores can be ignored, which can also be confirmed from the EDS mapping images of the IL@UiO-66-NH_2-TMC membrane (Fig. S3b and c, ESI†). The distribution of the Zr element in the IL@UiO-66-NH_2-TMC membrane also proves that most of the MOF is located on the surface of PES, and a small amount of MOF enters the interior of the PES pore. Therefore, based on the above results, the effect of the MOF membrane inside the PES

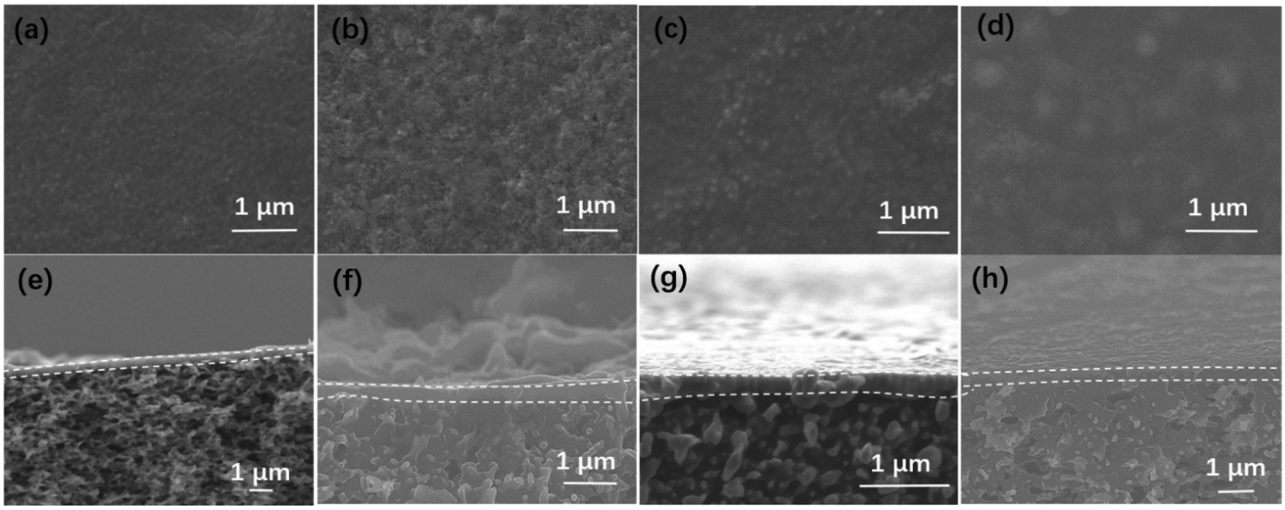

Fig. 5 The top-view SEM images of M0–M3 (a–d), and the cross-sectional SEM image of M0–M3 (e–h).

pores on the CO_2/CH_4 separation performance of the IL@UiO-66-NH_2-TMC membrane can be neglected.

TGA analysis was performed to further investigate the thermal performance of the IL-modified membrane (Fig. 6). M1–M3 membranes exhibited the first weight loss (43%, 54%, and 67%) at a temperature around 340 °C which could be attributed to the loss of IL in the membranes.[43,44] The IL loadings in M1–M3 membranes calculated from the TGA results were 0.17, 0.32, and 0.43 g, respectively, consistent with the amount of IL added during the experiment (Table 1). The second major weight loss started at a temperature of 500 °C which represented the decomposition of UiO-66-NH_2, which corresponds to the weight loss of M0 at 500–600 °C.[45,46] The third segment weight loss of M1–M3 membranes at a temperature of 600 °C can be regarded as the disintegration of PES. These results confirmed that both the composite membranes before and after modification exhibit ideal thermal stability for gas separation.

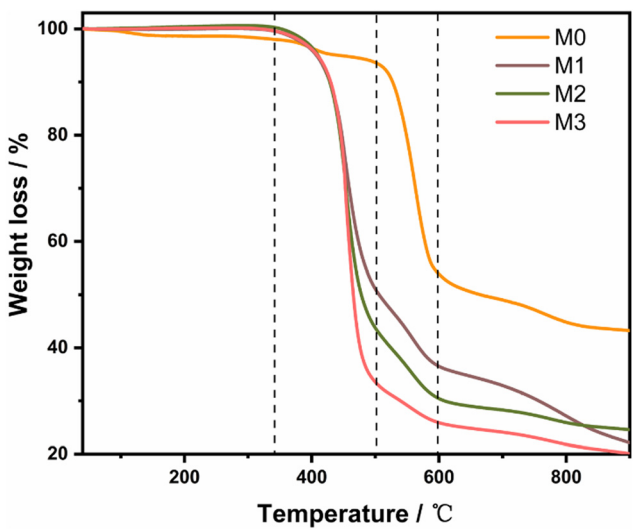

Fig. 6 TGA curves of M0–M3.

To illustrate the improvement of CO_2 adsorption capacity with the addition of ILs, the gas adsorption experiments were performed on the M0 membrane and M2 membrane with CO_2 and CH_4 at 298 K (Fig. 7). The adsorption capacities of the M0 membrane for CO_2 and CH_4 were 7.56 and 3.01 $cm^3\ g^{-1}$ at 298 K, while those of M2 membrane for CO_2 and CH_4 were 30.37 and 4.98 $cm^3\ g^{-1}$ at 298 K. The CO_2 adsorption ability of the M2 membrane is higher than that of the M0 membrane, proving that the addition of IL to the membrane can effectively improve the CO_2 adsorption capacity of the membrane.

3.2 Gas separation test

The successful assembly of ILs within the membranes and affinity between CO_2 and the IL inspired us to study the CO_2/CH_4 gas separation performance of the IL@UiO-66-NH_2-TMC membranes. The mixed gas (CO_2/CH_4 = 1/1, v/v) permeation tests were first performed on the PES, IL@PES, UiO-66-NH_2-TMC, and IL@UiO-66-NH_2-TMC membranes at room temperature under a pressure of 1.2 bar (Fig. 8a and Table S1, ESI†). The IL@PES exhibited a CO_2/CH_4 selectivity of 2.9, while that of PES is 0.59, indicating that the modification of the substrate with the IL could not achieve efficient separation of CO_2, and the selectivity is mainly due to the high CO_2 affinity of the IL. The selectivity of the UiO-66-NH_2-TMC membrane was only 0.98, corresponding to its large pore size of 1.15 nm. As expected, the CO_2/CH_4 selectivity of the IL@UiO-66-NH_2-TMC membrane was significantly improved to 35, compared with that of the IL@PES and UiO-66-NH_2-TMC membranes. The high CO_2/CH_4 selectivity is not only due to the excellent CO_2 adsorption ability for the IL (Fig. 7b) but also because the IL effectively occupies the interspace between the MOF and TMC monomers. These results indicate that the IL post-modified UiO-66-NH_2-TMC membrane is an effective strategy to improve the CO_2/CH_4 separation performance.

The assembled amount of IL has a significant effect on the gas separation performance of the membranes. As the IL concentration increased (from 10 to 30 wt%), a trend was observed for IL@UiO-66-NH_2-TMC membranes in which the

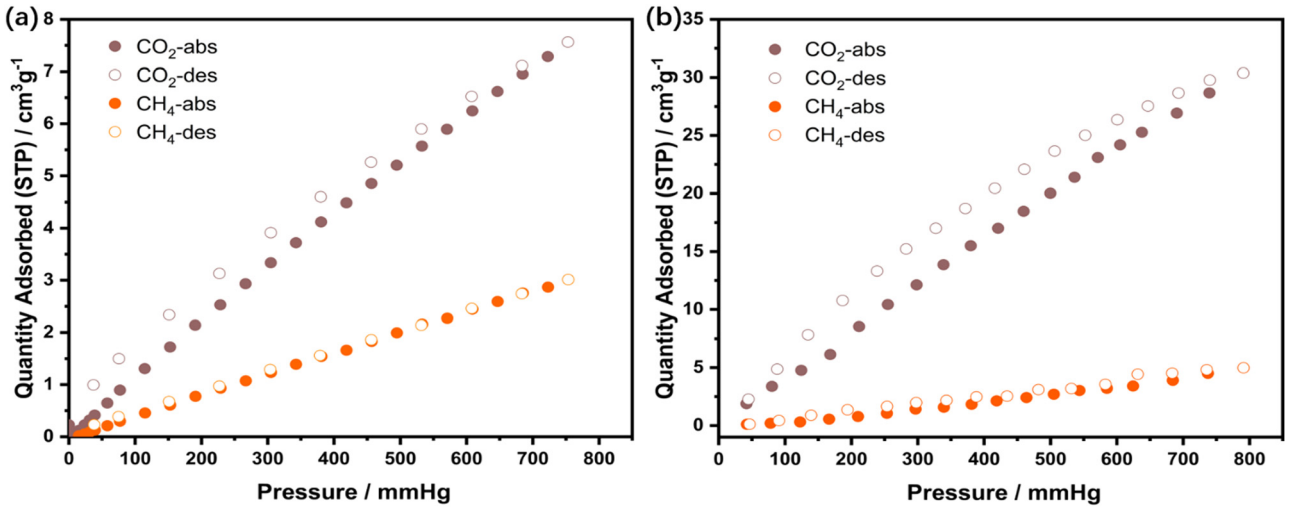

Fig. 7 (a) CO_2 and CH_4 adsorption–desorption isotherms of the M0 membrane at 298 K. (b) CO_2 and CH_4 adsorption–desorption isotherms of M2 membrane at 298 K.

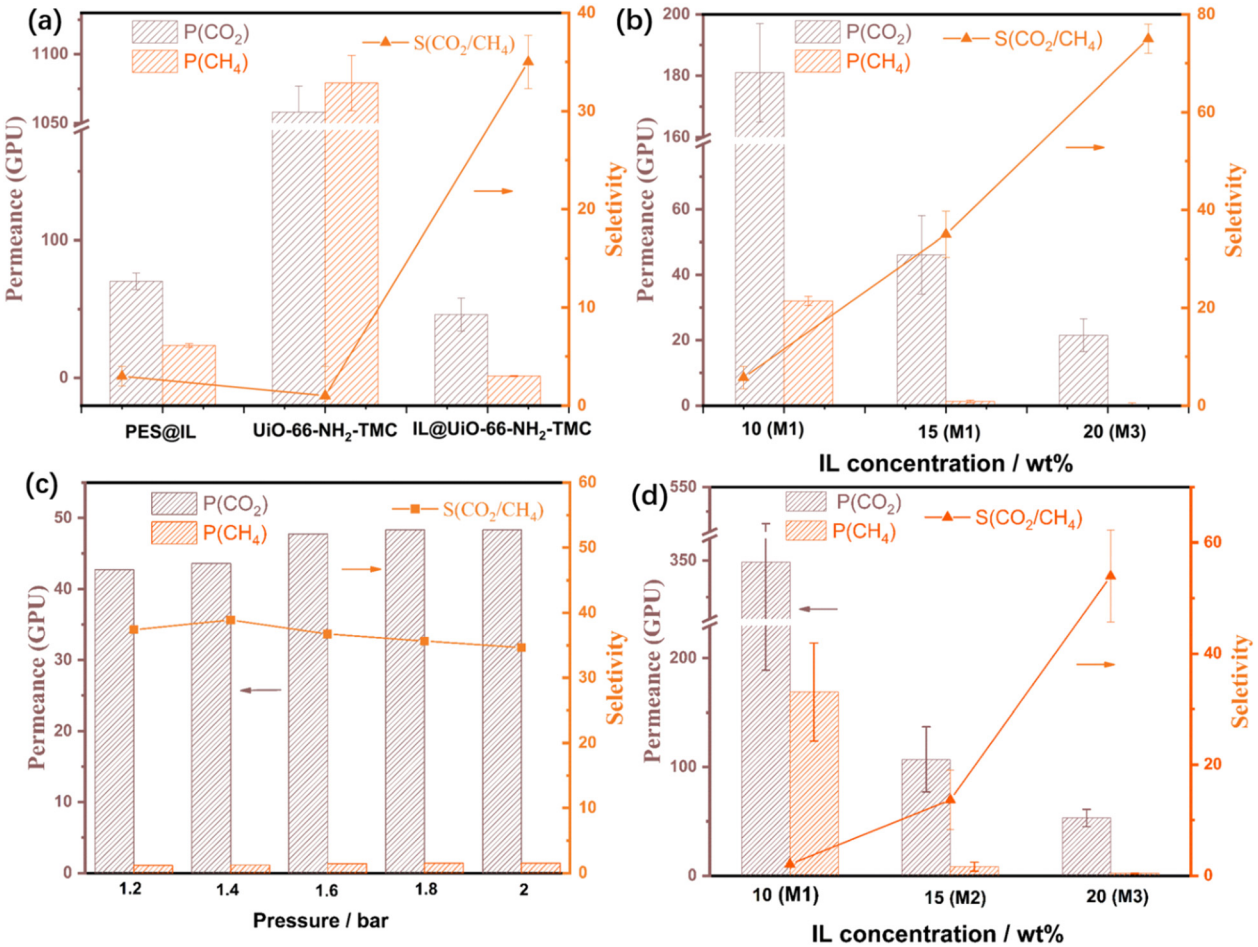

Fig. 8 (a) Mixed gas permeation properties of the PES@IL, UiO-66-NH_2-TMC, and IL@UiO-66-NH_2-TMC membrane at 25 °C. (b) Mixed gas permeation properties of the M1–M3 membranes at 25 °C. (c) Mixed gas permeation properties of the M2 membrane under different trans-membrane pressure drops. (d) Single gas permeation properties of the M1–M3 membranes at 25 °C.

CO_2/CH_4 separation selectivity increased and the CO_2 permeance decreased (Fig. 8b). The M1 prepared with 10 wt% IL concentration has a high CO_2 permeance of 180 GPU but a low selectivity of 5.7. The lower IL concentration cannot fully fix the space between the MOF and TMC so the gas selectivity cannot be effectively improved. The M2 membrane exhibited a CO_2/CH_4 selectivity of 35 associated with a CO_2 permeability of 46 GPU, reflecting a substantial enhancement in CO_2/CH_4 selectivity as compared to the UiO-66-NH_2-TMC membrane (Fig. 8a). When the IL concentration reached 20 wt%, the membrane showed up to 75 separation selectivity for CO_2/CH_4, but considering its low gas permeance, a membrane with an IL concentration of 15 wt% was selected for the further gas separation test.

The mixed gas permeance for the M2 membrane under different trans-membrane pressure drops (1.2–2.0 bar) was also evaluated (Fig. 8c). As the pressure increases, the CO_2 permeance slightly increased (from 42 to 47 GPU) and the CO_2/CH_4 selectivity remained unchanged (35), indicating that the M2 membrane can maintain stable separation performance under different transmembrane pressure drops. The evaluated membranes sustained their associated performances, affirming that the IL@UiO-66-NH_2-TMC membrane has a defect-free selective layer that enables stable gas separation performance at different pressures. Under a trans-membrane pressure of 2 bar, we performed the gas separation test at 120 °C. The results (Table S2, ESI†) confirmed that the IL@UiO-66-NH_2-TMC membrane was stable under this condition and can maintain efficient separation performance.

The solution-diffusion model was applied to investigate the separation mechanism of the IL@UiO-66-NH_2-TMC membrane. To obtain the permeability of different gases, the single gas permeation tests for pure CO_2 (99.995%) and CH_4 (99.995%) under a pressure of 1.2 bar were performed on the IL@UiO-66-NH_2-TMC membrane (Fig. 8d). The composite membrane (M1–M3) possessed the higher CO_2/CH_4 selectivity (5.7, 35, and 75) of mixed gases than the ideal selectivity (2, 13.6, and 54), attributed to the competitive adsorption of CO_2 and CH_4 by the membranes.[47] The solubility (S) and diffusivity (D) for the M2 membranes are summarized in Table 2. The result shows that the selectivity of the membrane is more dependent on solubility ($S_{CO_2/SCH_4=5.9} > D_{CO_2}/D_{CH_4=2.2}$). It is much easier to adsorb CO_2 than CH_4 by the IL-modified composite membranes, declining the adsorption and diffusion of CH_4, thereby enhancing the separation selectivity.

To further investigate the stability of the IL@UiO-66-NH_2-TMC membrane, the gas separation performance of the membrane was continuously tested at a trans-membrane pressure of 1.2 bar (Fig. 9). The CO_2/CH_4 selectivity of 36 remained unchanged after continuous 1440-min gas separation tests,

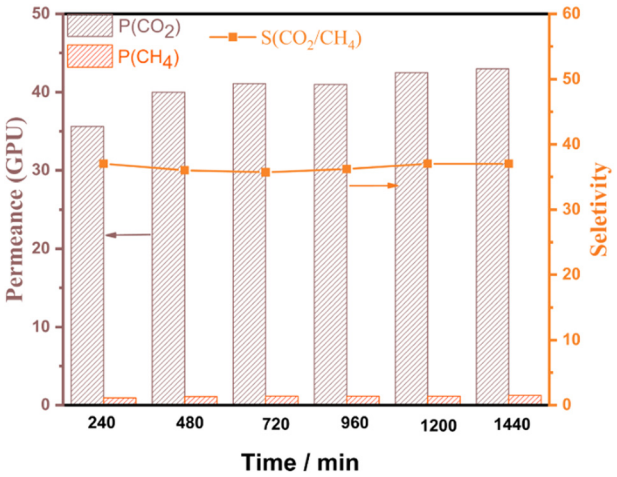

Fig. 9 The plot of CO_2/CH_4 permeance and selectivity for the IL@UiO-66-NH_2-TMC membrane *versus* test time.

demonstrating the excellent stability of the membrane. The firm assembly of the IL within the membrane is influenced by several factors: (i) the F atoms in the IL generate hydrogen bonding interactions with the UiO-66-NH_2-TMC membrane; (ii) the very small interspace (1.15 nm) between the MOF and TMC monomers can effectively bind the imidazolium cations in the ionic liquid and prevent their detachment from the interior of the membrane.[24]

3.3 Comparison of the reported UiO-66 based membranes

Fig. 10 shows the comparison of separation performances for the IL@UiO-66-NH_2-TMC membrane and reported other state-of-the-art UiO-66 based polycrystalline and composite membranes together with 2008 Robeson upper bounds. The synthesized IL@UiO-66-NH_2-TMC membranes exhibit significantly enhanced CO_2 selectivity over the UiO-66-NH_2-TMC membrane, proving that the IL post-modification strategy is an effective means to obtain high-performance CO_2 separation membranes. In addition, compared with the state-of-the-art UiO-66 based polycrystalline and composite membranes reported in the literature, the membranes synthesized in this work exhibit higher CO_2 separation performance and are close to Robson's upper bound. Hence, this comparison study revealed that the IL@UiO-66-NH_2-TMC membranes fabricated in the present work are potential for CO_2 separation processes.

4. Conclusions

In summary, we demonstrate that ILs acting as cavity occupants is a facile and efficient method to trigger the CO_2/CH_4 separation performance of MOF-based composite membranes. The addition of ILs with high CO_2 affinity filled the interspace between the

Table 2 The value of solubility (S) and diffusivity (D) for the M2 membrane at 298 K

Membrane	S_{CO_2} (mol m^{-3} Pa^{-1})	S_{CH_4} (mol m^{-3} Pa^{-1})	S_{CO_2}/S_{CH_4}	D_{CO_2} (m^2 s^{-1})	D_{CH_4} (m^2 s^{-1})	D_{CO_2}/D_{CH_4}
M2	4.9×10^{-3}	8.3×10^{-4}	5.9	7.3×10^{-13}	3.3×10^{-13}	2.2

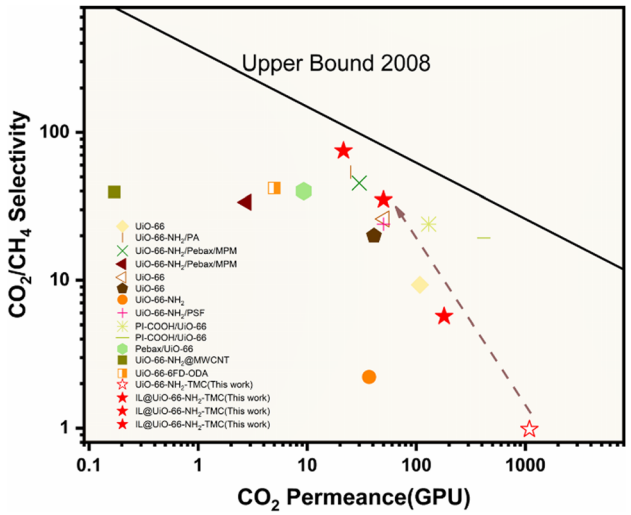

Fig. 10 Comparison of the CO_2/CH_4 separation performances between the IL@UiO-66-NH_2-TMC membranes prepared in this study and other UiO-66 polycrystalline and composite membranes reported in the literature. Upper bound front drawn assuming a membrane thickness of 1 μm. Detailed information in this figure is listed in Table S3 (ESI†).

MOF and TMC monomers, resulting in a significant increase in the CO_2/CH_4 selectivity (35) compared to that of the pristine membrane (0.98). The hydrogen bond interaction between the IL and MOF composite membranes solved the problem of IL loss and improved the separation stability of the membrane. The preparation of MOF composite membranes by the interfacial assembly method and the functional modification of ILs provide new opportunities to design flexible, high filler proportions, ultrathin, and scalable MOF-based membranes for gas separation.

Author contributions

Xiaolei Cui: conceptualization, writing – original draft, and data curation. Zixi Kang: conceptualization, funding acquisition, writing – review & editing, and supervision. Weidong Fan: investigation. Jia Pang: formal analysis and supervision. Yang Feng: software and supervision. Caiyan Zhang: software and formal analysis. Liting Yu: data curation and validation. Shuo Liu: data curation and validation. Xiuxian Tang: visualization. Lili Fan: validation. Rongming Wang: validation. Daofeng Sun: funding acquisition and supervision.

Conflicts of interest

There are no conflicts to declare.

Acknowledgements

This work was supported by the National Natural Science Foundation of China (Grants No. 22171288), the Key Research and Development Projects of Shandong Province (2019JZZY010331), the Shandong Province Natural Science Foundation (ZR2020MB017), the Fundamental Research Funds for the Central Universities (RA2008003) and the Outstanding Youth Science Fund Projects of Shandong Province (2022HWYQ-070).

References

1 S. Wang, X. Li, H. Wu, Z. Tian, Q. Xin, G. He, D. Peng, S. Chen, Y. Yin, Z. Jiang and M. D. Guiver, Advances in high permeability polymer-based membrane materials for co_2 separations, *Energy Environ. Sci.*, 2016, **9**, 1863–1890.

2 Z. Cheng, S. Li, Y. Liu, Y. Zhang, Z. Ling, M. Yang, L. Jiang and Y. Song, Post-combustion co_2 capture and separation in flue gas based on hydrate technology: a review, *Renewable Sustainable Energy Rev.*, 2022, **154**, 111806.

3 H. Yang and W. Ho, Polymeric membranes for CO_2 separation and capture, *J. Membr. Sci.*, 2021, **628**, 119244.

4 X. Chen, G. Liu and W. Jin, Natural Gas Purification by Asymmetric Membranes: An Overview, *Green Energy Environ.*, 2021, **6**, 176–192.

5 X. S. Li, C. G. Xu, Z. Y. Chen and H. J. Wu, Tetra-*n*-Butyl ammonium bromide semi-clathrate hydrate process for post-combustion capture of carbon dioxide in the presence of dodecyl trimethyl ammonium chloride, *Energy*, 2010, **35**, 3902–3908.

6 S. Basu, A. L. Khan, A. Cano-Odena, C. Liu and I. F. J. Vankelecom, Membrane-based technologies for biogas separations, *Chem. Soc. Rev.*, 2010, **39**, 1–19.

7 M. Rezakazemi, A. Ebadi Amooghin, M. M. Montazer-Rahmati, A. F. Ismail and T. Matsuura, State-of-the-art membrane-based CO_2 separation using mixed matrix membranes (MMMs): An overview on current status and future directions, *Prog. Polym. Sci.*, 2014, **39**, 817–861.

8 G. Chen, T. Wang, G. Zhang, G. Liu and W. Jin, Membrane materials targeting carbon capture and utilization, *Adv. Membr.*, 2022, **2**, 100025.

9 J. Yu, L. H. Xie, J. R. Li, Y. Ma and P. B. Balbuena, CO_2 Capture and Separations Using MOFs: Computational and Experimental Studies, *Chem. Rev.*, 2017, **117**, 9674–9754.

10 L. Yang, S. Qian, X. Wang, X. Cui, B. Chen and H. Xing, Energy-efficient separation alternatives: metal–organic frameworks and membranes for hydrocarbon separation, *Chem. Soc. Rev.*, 2020, **49**, 5359–5406.

11 B. Ghalei, K. Sakurai, Y. Kinoshita, K. Wakimoto, A. Isfahani, Q. Song, K. Doitomi, S. Furukawa, H. Hirao and H. Kusuda, Enhanced selectivity in mixed matrix membranes for CO_2 capture through efficient dispersion of amine-functionalized MOF nanoparticles, *Nat. Energy*, 2017, **2**, 1–9.

12 M. Kalaj, K. C. Bentz, S. Ayala, J. M. Palomba and S. M. Cohen, MOF-polymer hybrid materials: from simple composites to tailored architectures, *Chem. Rev.*, 2020, **120**, 8267–8302.

13 Y. Katayama, M. Kalaj, K. S. Barcus and S. M. Cohen, Self-assembly of metal-organic framework (MOF) nanoparticle monolayers and free-standing multilayers, *J. Am. Chem. Soc.*, 2019, **141**, 20000–20003.

14 Y. Zhang, X. Feng, H. Li, Y. Chen, J. Zhao, S. Wang, L. Wang and B. Wang, Photoinduced postsynthetic polymerization

of a metal-organic framework toward a flexible stand-alone membrane, *Angew. Chem., Int. Ed.*, 2015, **54**, 4259–4263.
15 X. Cui, G. Kong, Y. Feng, L. Li, W. Fan, J. Pang, L. Fan, R. Wang, H. Guo, Z. Kang and D. Sun, Interfacial polymerization of MOF ''monomers'' to fabricate flexible and thin membranes for molecular separation with ultrafast water transport, *J. Mater. Chem. A*, 2021, **9**, 17528–17537.
16 O. Tzialla, Ch Veziri, X. Papatryfonl and K. G. Beltsios, Zeolite Imidazolate Framework–Ionic Liquid Hybrid Membranes for Highly Selective CO_2 Separation, *J. Phys. Chem. C*, 2013, **117**, 18434–18440.
17 J. Li, H. Lian, K. Wei, E. Song and W. Xing, Synthesis of tubular ZIF-8 membranes for propylene/propane separation under high-pressure, *J. Membr. Sci.*, 2019, **595**, 117503.
18 R. Zhou, H. Wang, B. Wang, X. Chen, S. Li and Y. Miao, Defect-Patching of Zeolite Membranes by Surface Modification Using Siloxane Polymers for CO_2 Separation, *Ind. Eng. Chem. Res.*, 2015, **54**, 7516–7523.
19 G. Durga, P. Kalra, V. K. Verma, K. Wangdi and A. Mishra, Ionic liquids: From a solvent for polymeric reactions to the monomers for poly (ionic liquids), *J. Mol. Liq.*, 2021, **335**, 116540.
20 Z. Lei, C. Dai and B. Chen, Gas solubility in ionic liquids, *Chem. Rev.*, 2014, **114**, 1289–1326.
21 S. S. D. Jesus and R. M. Filho, Are ionic liquids eco-friendly?, *Renewable Sustainable Energy Rev.*, 2022, **157**, 112038.
22 S. Zemg, X. P. Zhang, L. Bai, X. Zhang, H. Wang, J. Wang, D. Bao, M. Li, X. Liu and S. Zhang, Ionic-Liquid-Based CO_2 Capture Systems: Structure, Interaction and Process, *Chem. Rev.*, 2017, **117**, 9625–9673.
23 L. C. Tomé and I. M. Marrucho, Ionic liquid-based materials: a platform to design engineered CO_2 separation membranes, *Chem. Soc. Rev.*, 2016, **45**, 2785–2824.
24 Y. Ban, Z. Li, Y. Li, Y. Peng, H. Jin, W. Jiao, A. Guo, P. Wang, Q. Yang and C. Zhong, Confinement of Ionic Liquids in Nanocages: Tailoring the Molecular Sieving Properties of ZIF-8 for Membrane-Based CO_2 Capture, *Angew. Chem., Int. Ed.*, 2015, **54**, 15483–15487.
25 Y. Gong, S. Gao, Y. Tian, Y. Zhu and J. Jin, Thin-film nanocomposite nanofiltration membrane with an ultrathin polyamide/UIO-66-NH_2 active layer for high-performance desalination, *J. Membr. Sci.*, 2020, **600**, 117874.
26 Y. Feng, Z. Wang, W. Fan, Z. Kang, S. Feng, L. Fan, S. Hu and D. Sun, Engineering the pore environment of metal–organic framework membranes via modification of the secondary building unit for improved gas separation, *J. Mater. Chem. A*, 2020, **8**, 13132–13141.
27 S. Feng, M. Bu, J. Pang, W. Fan and D. Sun, Hydrothermal stable ZIF-67 nanosheets via morphology regulation strategy to construct mixed-matrix membrane for gas separation, *J. Membr. Sci.*, 2020, **539**, 117404.
28 W. J. Koros and C. Zhang, Materials for next-generation molecularly selective synthetic membranes, *Nat. Mater.*, 2017, **16**, 289–297.
29 D. Saha, R. Sen, T. Maity and S. Koner, Anchoring of palladium onto surface of porous metal-organic framework through post-synthesis modification and studies on Suzuki and Stille coupling reactions under heterogeneous condition, *Langmuir*, 2013, **29**, 3140–3151.
30 H. Rajati, A. H. Navarchian, D. Rodrigue and S. Tangestaninejad, Effect of immobilizing ionic liquid on amine-functionalized MIL-101(Cr) incorporated in Matrimid membranes for CO_2/CH_4 separation, *Chem. Eng. Process.*, 2021, **168**, 108590.
31 J. Lu, X. Zhang, L. Xu, G. Zhang and Q. Meng, Preparation of amino-functional UiO-66/PIMs mixed matrix membranes with [bmim][Tf_2N] as regulator for enhanced gas separation, *Membranes*, 2021, **11**, 35.
32 B. Sasikumar and G. Arthanareeswaran, Interfacial design of polysulfone/Cu-BTC membrane using [Bmim][Tf_2N] and [Dmim][Cl] RTILs for CO_2 separation: Performance assessment for single and mixed gas separation, *Sep. Purif. Technol.*, 2022, 121315.
33 Y. Zhao, D. Wang, W. Wei, L. Cui, C. Cho and G. Wu, Effective adsorption of mercury by Zr (IV)-based metal-organic frameworks of UiO-66-NH_2 from aqueous solution, *Environ. Sci. Pollut. Res.*, 2021, **28**, 7068–7075.
34 F. Zhao, C. Su, W. Yang, Y. Han and Z. Li, In-situ Growth of UiO-66-NH_2 onto Polyacrylamide-Grafted Nonwoven Fabric for Highly Efficient Pb(II) Removal, *Appl. Surf. Sci.*, 2020, **527**, 146862.
35 B. Sasikumar and G. Arthanareeswaran, Interfacial design of polysulfone/Cu-BTC membrane using [Bmim][Tf_2N] and [Dmim][Cl] RTILs for CO_2 separation: Performance assessment for single and mixed gas separation, *Sep. Purif. Technol.*, 2022, **295**, 121315.
36 Y. Wu, Y. Xiao, H. Yuan, Z. Zhang and G. Xiao, Imidazolium ionic liquid functionalized UiO-66-NH_2 as highly efficient catalysts for chemical fixation of CO_2 into cyclic carbonates, *Microporous Mesoporous Mater.*, 2021, **310**, 110578.
37 H. Rajati, A. H. Navarchian, D. Rodrigue and S. Tangestaninejad, Effect of immobilizing ionic liquid on amine-functionalized MIL-101(Cr) incorporated in Matrimid membranes for CO_2/CH_4 separation, *Chem. Eng. Process.*, 2021, **168**, 108590.
38 Y. H. Lee, S. H. Han and Y. S. Kim, Investigation of hydrophobic properties of PSII-modified EVOH, LLDPE, and PET Films, *J. Surf. Anal.*, 2015, **12**, 258.
39 P. K. Wu and T. M. Lu, Metal/polymer adhesion enhancement by reactive ion assisted interface bonding and mixing, *Appl. Phys. Lett.*, 1997, **71**, 2710–2712.
40 T. Hammer, M. Reichelt and H. Morgner, Influence of the aliphatic chain length of imidazolium based ionic liquids on the surface structure, *Phys. Chem. Chem. Phys.*, 2010, **12**, 11070–11080.
41 M. Sobota, M. Schmid, M. Happel, M. Amende, F. Maier, H.-P. Steinrück, N. Paape, P. Wasserscheid, M. Laurin and J. M. Gottfried, Ionic liquid-based model catalysis: interaction of [BMIM][Tf_2N] with Pd nanoparticles supported on an ordered alumina flm, *Phys. Chem. Chem. Phys.*, 2010, **12**, 10610–10621.
42 M. A. Molina, N. R. Habib, I. Díaz and S. Manuel, Surfactant-induced hierarchically porous MOF-based catalysts prepared under sustainable conditions and their ability to remove bisphenol A from aqueous solutions, *Catal. Today*, 2022, **394**, 117–124.
43 S. Kavak, H. M. Polat, H. Kulak, S. Keskin and A. Uzun, MIL-53(Al) as a Versatile Platform for Ionic-Liquid/MOF

Composites to Enhance CO_2 Selectivity over CH_4 and N_2, *Chem. – Asian J.*, 2019, **14**, 3655–3667.

44 N. N. R. Ahmad, C. P. Leo, A. W. Mohammad and A. L. Ahmad, Interfacial sealing and functionalization of polysulfone/SAPO-34 mixed matrix membrane using acetate-based ionic liquid in post-impregnation for CO_2 capture, *Sep. Purif. Technol.*, 2018, **197**, 439–448.

45 H. Guo, J. Liu, Y. Li, J. Caro and A. Huang, Post-synthetic modification of highly stable UiO-66-NH_2 membranes on porous ceramic tubes with enhanced H_2 separation, *Microporous Mesoporous Mater.*, 2021, **313**, 110823.

46 M. Vahidi, A. Tavasoli and A. M. Rashidi, Preparation of amine functionalized UiO-66, mixing with aqueous N-Methyldiethanolamine and application on CO_2 solubility, *J. Nat. Gas Sci. Eng.*, 2016, **28**, 651–659.

47 B. Liu, R. Zhou, N. Bu, Q. Wang, S. Zhong, B. Wang and K. Hidetoshi, Room-temperature ionic liquids modified zeolite SSZ-13 membranes for CO_2/CH_4 separation, *J. Membr. Sci.*, 2017, **524**, 12–19.

